# Chapter 6
# Laser Microporation of Skin

The percutaneous permeation of drugs across the skin is greatly enhanced when the stratum corneum (SC) is compromised by physical poration. The presence of pores allows even the transport of larger molecules, such as proteins, peptides and vaccines, across the skin [1, 2]. Exposure to laser radiation can be used to ablate the skin and form pores. The mechanism of ablation depends on the wavelength and pulse duration of the laser used.

Currently, devices available for laser microporation of the skin are used both for drug delivery and cosmetic applications [1, 3]. The pulse durations involved are in the microsecond range and ablate the skin photothermally; the water within the skin absorbs the laser light and vaporizes, causing ablation. However, the lasers required are expensive and their use is associated with side effects, such as skin irritation and a prolonged healing period [4, 5].

Ablation of skin using visible laser light has been less studied and requires a higher fluence for ablation and permeation enhancement compared to infrared (IR) and ultraviolet (UV) lasers [6, 7]. The use of visible light, however, is safer as unintentional exposure is easily observed and can therefore be controlled. Demonstrations of skin ablation using a femtosecond pulsed laser indicated that the mechanism involved plasma formation [8–10]. Histological examination of the skin after exposure to the laser beam revealed some tissue damage around the ablated pore but, due to its shorter pulse duration, femtosecond ablation has the potential to cause much less thermal perturbation than microsecond pulsed devices. Femtosecond ablation of porcine mammalian has therefore been investigated here, with a view to decreasing the fluence required for ablation and therefore limiting the extent of thermal damage.

Porcine skin has been porated using a fibre laser with a wavelength of 532 nm and pulse durations of approximately 300 fs. A dye was applied to the surface of the skin, enabling the use of lower laser power. The ability of this ablation technique to enhance drug permeation across the SC was investigated with caffeine as a model drug. At lower powers, when poration was facilitated by the ink on the surface of the skin, less thermal damage, as determined using Raman spectroscopy, was observed in the tissue surrounding the pores. The diameters of the pores could be varied by



H. Garvie-Cook, *Novel (Trans)dermal Drug Delivery Strategies*,
Springer Theses, DOI 10.1007/978-3-319-28901-4_6

changing the laser power and the distance between the skin and the fibre used to direct the light towards the skin. Greater enhancement in the permeation of caffeine was observed with increasing laser power. The use of both a fibre laser, and a fibre to direct the laser light towards the skin, allows for flexibility in the design of a portable device for laser microporation.

## 6.1 Pore Dimensions

Porcine skin was porated either without the application of an ink (uninked) or shortly after ink was applied to its surface (inked). The laser light was focussed on the skin using a lens (lens set-up) or directed to the skin using a fibre (fibre set-up).

### *6.1.1 Optical Microscopy of Laser Micropores*

Examples of pores formed by focussing laser light onto inked and uninked skin using a lens are shown in Fig. 6.1. The appearance of burnt tissue in uninked skin was clear, in Fig. 6.1a, b, around the sides and at the bottom of the pore. The occurrence of tissue damage in inked skin was less obvious (Fig. 6.1e, f) and the bottom of the pores was similar in appearance to the undamaged skin surrounding the pore. The lack of obvious thermal damage may reflect the fact that the black ink obscures visualisation of black, burnt tissue. Alternatively, it may be the case that there really is less damage to the tissue when the skin is inked. The pore in inked skin shown in Fig. 6.1e was formed using a lower power than that in uninked skin (Fig. 6.1a) (0.7 W as opposed to 1.3 W) which should result in less thermal damage. The ink influences the mechanism of poration, causing in less damage to the surrounding tissue and is further discussed in Sect. 6.4.

Cross-sectional images (Fig. 6.1c–d and g–h) were obtained by slicing through the middle of pores using a surgical scalpel. The skin was then supported on its side (with the cut surface facing upwards) and examined with an optical microscope. The images of pores in uninked skin show burnt tissue at the top and sides of the pores. In contrast, tissue burn in inked skin was again less obvious.

Laser light was also directed to the skin using a hollow core photonic crystal fibre (PCF). This fibre was specifically designed to guide femtosecond pulsed light with a wavelength of 532 nm, as used in these investigations. Fibres with air cores allow light with such short pulses to be guided without distortion. In more standard, silica fibres, nonlinear effects would alter the pulse and the high peak powers may cause damage [11].

An example of a pore produced by directing laser light to the skin using a fibre is shown in Fig. 6.2. Pores in inked skin were similar in appearance to those produced using the lens set-up but lower powers were used, resulting in smaller pores. The

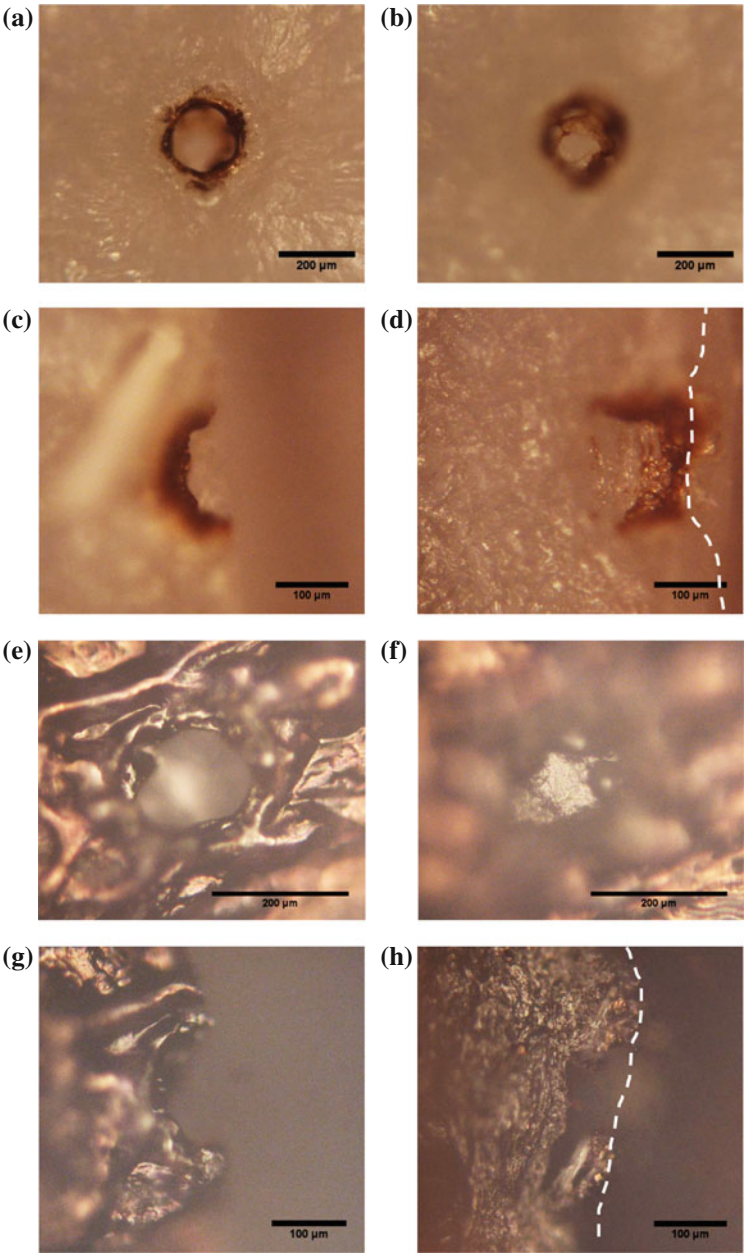


**Fig. 6.1** Optical microscopy images of laser pores in uninked **a**–**d** and inked skin **e**–**h**, produced by focussing laser light onto the skin using a lens. The microscope was focussed on the *top* (**a** and **e**) and bottom (**b** and **d**) of the pores. Cross section images were taken from the top down (**c** and **g**) and from the side (**d** and **h**). *White dashed lines* mark the uppermost surface of the skin. Laser powers of 1.0 W (**a** and **b**), 1.3 W (**c** and **d**) and 0.7 W (**e**–**h**) were used. Each row of images is obtained from a different pore. The exposure time to the laser was 1 s

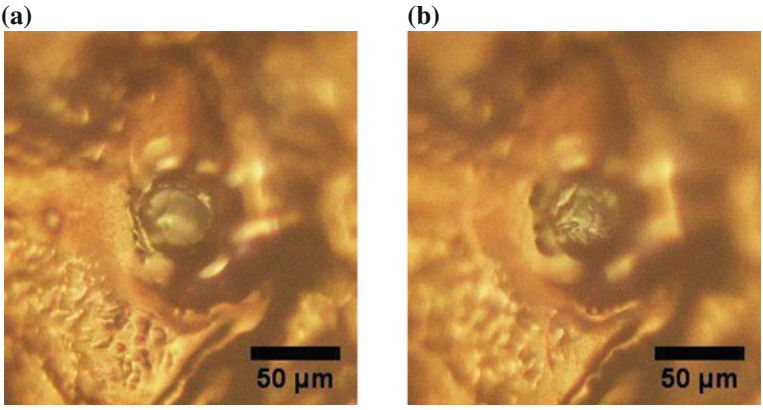


**Fig. 6.2** Optical microscopy images of the *top* (**a**) and *bottom* (**b**) of a pore in inked skin, formed by directing laser light onto the skin using a photonic crystal fibre. Images are taken from the top down. A laser power of 0.1 W was used to porate the skin. The exposure time to the laser was 1 s

bottom of the pore (Fig. 6.2a) does not appear to be burnt. A method was established, using Raman spectroscopy, to determine the extent of thermal damage after microporation. This is further described in Sect. 6.2.

### *6.1.2 Variation of Pore Dimensions*

The laser power $P$ (measured after the focussing optics as an average over 1 s), used to produce pores in both inked and uninked skin, was varied to determine its effect on the dimensions (diameter and depth) of the pores. The diameter of pores produced in both lens and fibre set-ups increased with increasing laser power (Fig. 6.3) and, in general, the pores became deeper. Using the lens set up, the dimensions of pores formed in inked and uninked skin were similar at the same power.

A threshold effect was apparent with respect to laser power, with different poration thresholds observed for pores produced using the lens and fibre set-ups. The threshold was the highest, at 0.7 W, for the production of pores in uninked skin. Below this threshold, no effect of laser illumination, under the same exposure conditions, was observed. The use of ink on the surface of the skin brought this threshold down to 0.2 W for pores produced using the lens set-up.

The use of the fibre set-up facilitated a further reduction in the threshold for poration to 0.05 W. The maximum power achievable at the surface of the skin was lower using the fibre set-up (0.4 W) than that using the lens set-up due to coupling losses when aligning the laser beam with the fibre. Pores were therefore not observed in uninked skin using the fibre set-up because the maximum power was too low to cause poration. The pores produced using the fibre set-up were smaller in diameter than those produced using the currently available P.L.E.A.S.E.® device [2], implying that they would be quicker to heal.

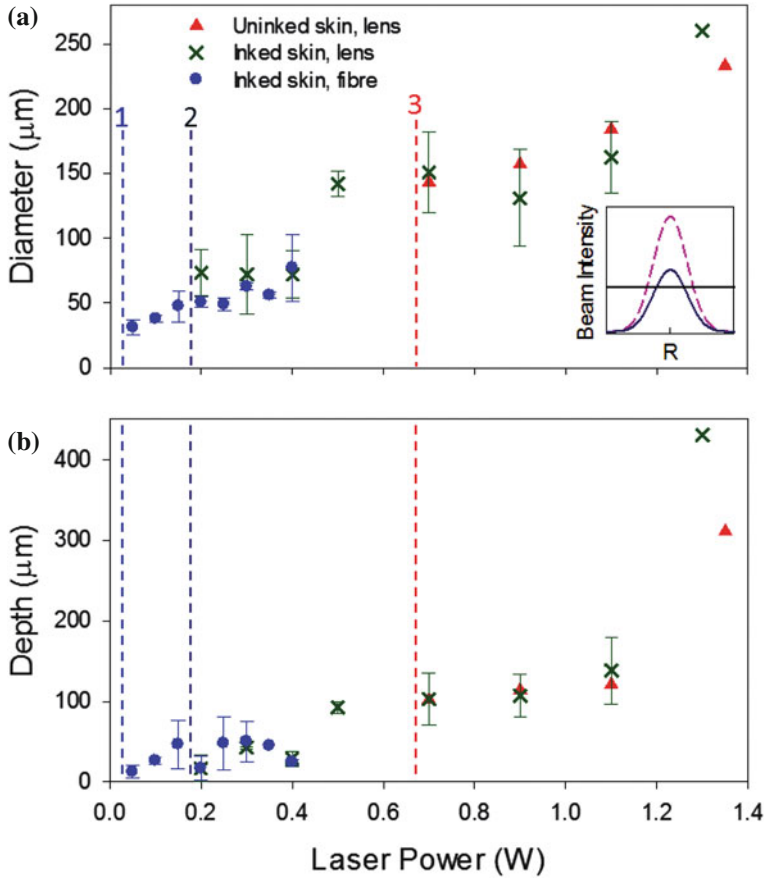


**Fig. 6.3** Laser pore diameter (**a**) and depth (**b**) as a function of the laser power used. Dimensions and poration thresholds are shown for pores produced on uninked and inked skin using a lens to focus the laser light onto the skin (*red* and *green symbols* and *dashed lines 3* and *2*, respectively) and on inked skin using a fibre to direct the laser light (*blue circles* and *dashed line 1*). Exposure times of 1 s were used. Averages (±standard deviation) were calculated from three pores on inked skin, except that produced at 1.3 W, when one measurement was carried out. One pore at each power was produced in uninked skin. The distance between the skin and the lens/fibre was kept constant. Beam intensities at high (*dashed pink*) and low powers (*blue*) at a given axial distance, calculated using Eq. 6.3, as a function of radial distance from the centre of the beam, are shown in the inset. A threshold value is shown (*black line*) to compare the diameter of pores at high and low powers

### *6.1.3 Beam Propagation*

Laser microporation using the lens set-up was not easy to reproduce. The incidence of poration was unreliable; the equipment would appear to be set up in the same way as previously but sometimes no poration was observed. This is likely to be due to the difficulty of accurately focussing the beam on the rough surface of the skin.

Laser beams often occur in the form of Gaussian beams [12]. Laser light focussed by a lens converges to its lowest diameter at the beam waist. It then diverges, at an angle which is dependent on the numerical aperture (NA) of the lens (in this case, 0.4), as the axial distance from the lens increases. A beam waist with a small radius can be obtained by focussing a laser beam using a lens with a high NA. The Gaussian beam emitted by the fibre initially has a beam radius dependent on the fibre's core diameter and then diverges according to the fibre's NA (0.04). The beam propagation from the lens and from the fibre has been modelled using the following equations.

The fluence of laser poration, the energy per unit area per exposure, is calculated using the following relation,

$$fluence = \frac{laser\ \ pulse\ energy}{effective\ \ focal\ \ spot\ \ area} \tag{6.1}$$

Fluence is commonly reported in similar experiments as it provides a measure of the safety of the exposure [12]. Due to the challenge of locating the exact position of the skin in relation to the beam waist in the case of the lens (and the large divergence of the beam away from the waist), the effective focal spot area is difficult to determine with high accuracy. For the results shown in Fig. 6.3, the distance between the lens and the outermost surface of the skin was kept constant, at approximately 2 mm, while the power was varied. The variation in power is therefore proportional to the variation in fluence.

The radius $\omega$ at which the intensity of a Gaussian beam drops to $\frac{1}{e^2}$ of its axial value as a function of the axial distance $z$ is given by Eq. 6.2 [12],

$$\omega(z) = \omega_0 \sqrt{1 + \left(\frac{z}{z_R}\right)^2} \tag{6.2}$$

where the minimum radius, the waist size, $\omega_0 = \frac{\lambda}{nNA}$, where $NA$ is the numerical aperture of the lens, $\lambda$ is the wavelength of the light and the Rayleigh range $z_R = \frac{\pi\omega_o^2}{\lambda}$. The beam emitted from the end of the fibre is assumed to have a waist size equal to the radius of the core of the fibre, 8 μm. The intensity $I$ of a Gaussian beam at an axial distance $z$ and radial distance $r$ is related to the intensity at the centre of the beam at its waist $I_0$ [12]:

$$I(r, z) = I_0 \left(\frac{\omega_0}{\omega(z)}\right)^2 \exp\left(\frac{-2r^2}{\omega^2(z)}\right) \tag{6.3}$$

where

$$I_0 = \frac{P_{peak}}{\pi\omega_0^2} \tag{6.4}$$

and the peak power for soliton pulses, as used in these experiments, $P_{peak} = 0.88\frac{P}{R\tau}$, where $R$ is repetition rate and $\tau$ is pulse duration [12].

Beam propagation from the lens and from the fibre, calculated using Eqs. 6.2, 6.3 and 6.4, is shown in Fig. 6.4a. Due to the existence of a threshold for ablation and the divergence of the beams (Fig. 6.4a), there is a limited range of distances over which poration can occur. Before or after this range, the fluence is below the threshold for ablation. Poration was therefore heavily dependent on the position of the skin relative to the lens but less so when the fibre was used, due to its lower NA. Finding the focus of the lens (and the small range of distance for ablation) was difficult due to the skin's low absorption and significant scattering at 532 nm. Positioning the focus optimally on the skin for ablation was also complicated by the skin's roughness, caused by larger furrows in the range of 20–100 μm, and shorter and shallower secondary furrows (5–40 μm), as well as smaller scale structures [13].

The fibre set-up ensured the reliable incidence of microporation and more reproducible results than the lens set-up. Light diverges with a lower angle from the end of the fibre than the light beam diverging from the beam waist of the lens set-up. The intensities of the laser beam at distances of 30 and 100 μm from the beam waist and from the end of the fibre are shown in Fig. 6.4b. There is a slower decrease in beam intensity with distance from the fibre, allowing a greater range of distances over which poration can occur. The roughness of the skin and its position therefore influence poration less using the fibre set-up than the lens set-up.

The diameter of the modelled beam at these distances is less than the diameter of the pores observed in these experiments (Fig. 6.3). The strong scattering of light by the skin [10] is likely to have increased the effective diameter of the beam. Optical scattering of light by the skin arises from spatial variation of the refractive index within the skin due to its inhomogeneous structure. The distribution and size of the components of the skin (lipids, proteins, etc.) provide a highly scattering medium for light with a wavelength of 532 nm [14]. The situation is not easy to model due to the contribution of various factors. Each pulse is thought to ablate a certain amount of material, implying that subsequent pulses will ablate material with a different spatial structure to the previous one (i.e., as the pore depth increases). The increase in temperature associated with the formation of a plasma (as discussed in Sects. 2.4.2 and 6.4) also affects the optical absorption of skin [14]. The third factor complicating the interaction of the laser beam with the skin is the deviation of the edges of the beam from a Gaussian function at high fluences [10]. Modelling the beam propagating from the fibre and from the lens, without incorporation of the scattering coefficient, provides a measure of the beam properties as functions of the distance from the beam waist to the skin and of the laser power. Although the pore diameters were greater than the calculated beam waist diameters, the variation in pore diameter with laser power and fibre-laser distance (further described in Sect. 6.4) were successfully accounted for.

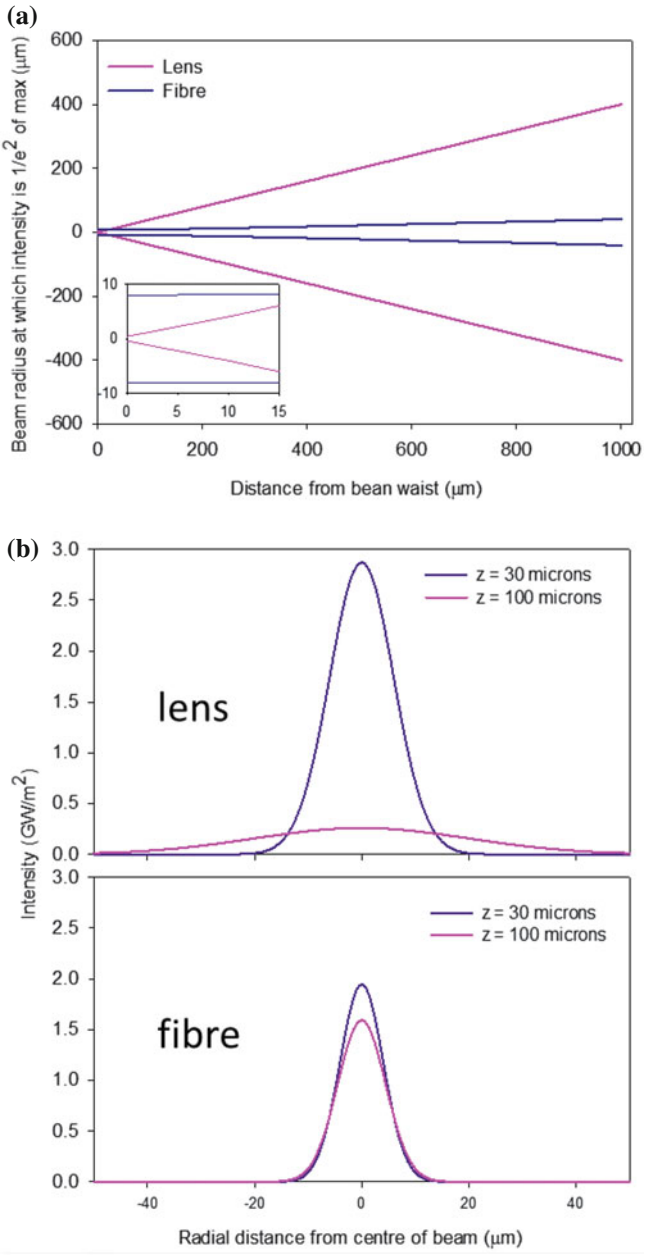


**Fig. 6.4** Gaussian beam divergence using the lens and fibre set-ups, calculated using Eq. 6.3: **a** beam radius as a function of axial distance from the lens (NA = 0.4) waist and from the end of the fibre (NA = 0.04), **b** intensity as a function of radial distance at axial distances of 30 and 100 μm using the lens and fibre set-ups. Intensity was calculated using the maximum power (1.3 W for lens, 0.4 W for fibre) and the cross-sectional areas of the beam waist of the lens, and of the fibre core, respectively

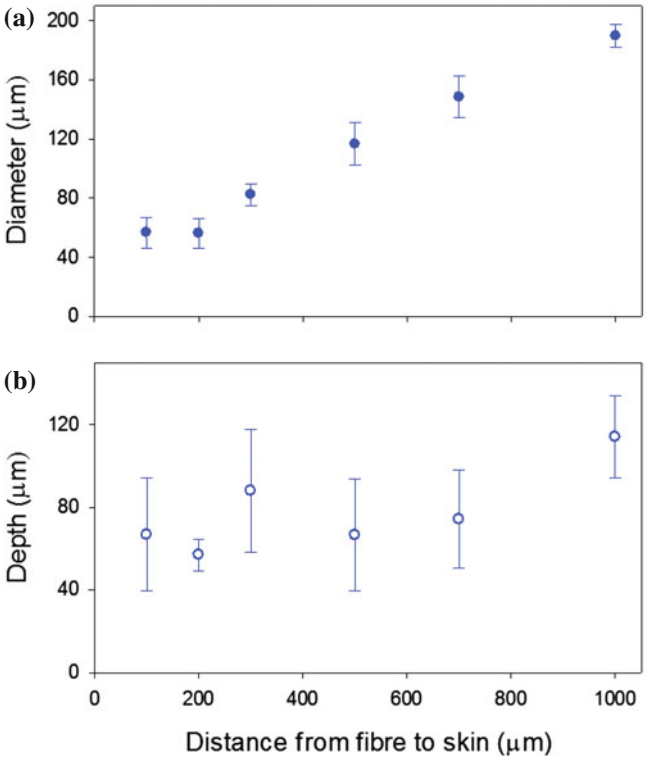


**Fig. 6.5** Laser pore diameter (**a**) and depth (**b**) as a function of the distance between the surface of the skin and the fibre used to direct laser light onto the skin. Exposure times of 1 s were used and power was kept constant at 0.3 W. Averages (±standard deviation) were calculated using five pores at each power on two porcine skin samples

### *6.1.4 Poration Using the Fibre Set-Up*

A low power for laser microporation, achievable using the fibre set-up, is useful in lowering the cost of the process. At lower powers, less heat is produced in the laser system so fewer components are needed to cool the system. Lower power emitted from the laser system would also improve its safety profile.

Once the fibre set-up was established, enabling reliable and predictable microporation to be achieved, further investigation of the pore dimensions were undertaken. The distance between the end of the fibre and the surface of the skin, and the amount of time that the skin was exposed to the laser beam, were varied.

Increasing the distance between the end of the fibre and the surface of the skin beyond 200 μm resulted in pores with larger diameters (Fig. 6.5). The surface of the skin was considered to be the outermost edge of tissue, observed using an optical microscope. As mentioned previously, the beam emitted from the fibre diverges

slowly, due to its low NA. As the distance between the fibre and the skin increases, the diameter of the diverging beam becomes larger, resulting in pores with greater diameters. Even though the fluence is smaller at a greater distance, poration is still possible at 1 mm away from the skin. There may be a threshold effect at greater distances when the fluence becomes too low for poration of inked skin.

There was no significant difference between the diameter of the pores at distances of 100 and 200 μm. There is little difference between the diameters of the beam at these distances too (Fig. 6.4a). Below 200 μm, pores of the same diameter are produced regardless of the roughness of the skin, which is prominent at these small distances. The diameter of the pores is therefore predictable regardless of the roughness of the skin, which should be useful when designing a device control drug delivery through this route.

The depth of the pores did not vary significantly with distance from the fibre to the skin although the error on these measurements is quite large. The variability may be due to inherent differences in the depths of the pores or to the method of measurement. Large variations in pore depth may occur because of the interaction of the laser light with hairs in the skin, for example, which absorb laser energy in a different way due to their pigmentation and structural characteristics. There may also be other regional variations in skin structure which influence the depth of the ablated pore. However, it is likely this would also affect the diameter of the pores although this appears not to be the case.

To measure depth, the top of a pore was brought into focus using an optical microscope. The vertical position of the skin was then adjusted until the bottom of the pore was in focus. The depth of the pore was determined as the difference in vertical position between the two foci. When the pores were large (for example, at large fibre-skin distances), the top of the pore was sometimes higher on one side than the other due to the roughness of the skin at these larger scales. It was therefore difficult to determine from which point the depth should be measured. The uppermost top edge was usually used, which may have led to an overestimation of the pore depth. Previous studies have used histology to determine the depth of laser pores and this presents an alternative [15, 16], and potentially more accurate, method. This does, however, require treatment and staining of the skin, which may affect the properties of the tissue and therefore the results observed.

There was no significant difference in the diameter or depth of the pores with exposure times in the range of 0.07–1 s (Fig. 6.6). This is in disagreement with previous studies [1, 17], which report that pore depth increased with the number of pulses used for poration. These studies, however, used much lower numbers of pulses than were obtainable in these experiments; 1–50, as opposed to the 1.4–20 million pulses achieved here. The pulse durations used in these previous studies were also longer, in the range of microseconds, suggesting that a different mechanism of poration may be operative. It is possible that a relation exists, at lower exposure times, between the dimensions of the pores and the exposure time used to produce them. The poration process is likely to have been completed more quickly than the shortest exposure time used, 0.07 s. The same depths were therefore observed for longer exposure times.

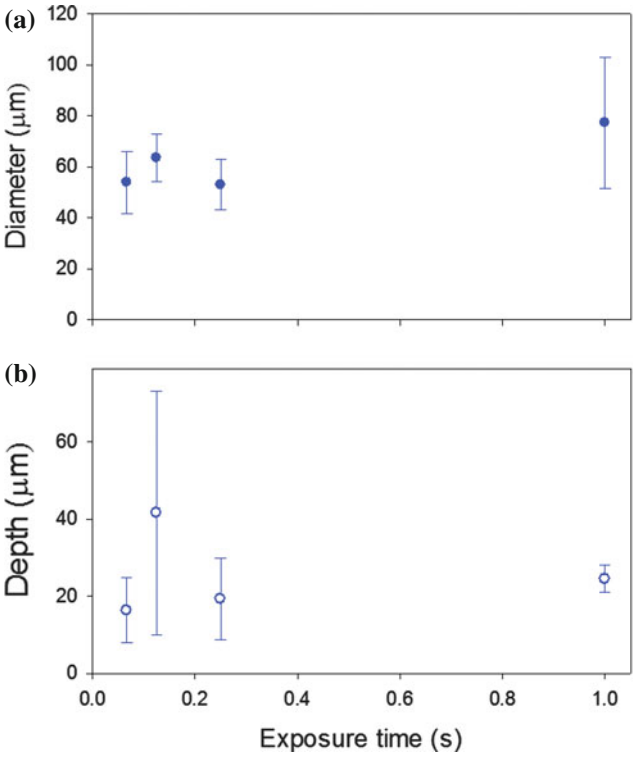


**Fig. 6.6** Laser pore diameter (**a**) and depth (**b**) as a function of the exposure time. Results are shown for pores produced on inked skin using a fibre to direct the laser light. The distance between the skin and the fibre, and the laser power (0.3 W), were kept constant

## 6.2 Raman Micro-Spectroscopy

Raman spectroscopy proved a useful tool to objectively determine thermal damage induced during poration via the fluorescence emitted by burnt tissue.

### *6.2.1 Thermal Damage Detection*

Raman spectra of porcine skin, which had suffered increasingly severe thermal damage, were acquired (Fig. 6.7). The skin was burnt using a soldering iron at different temperatures. The spectrum of skin burnt at 420 °C showed a large background fluorescence which was 5 orders of magnitude greater than the signal from unburnt skin. Some spectral features, characteristic of unburnt skin, were observed in skin which had been burnt at a lower temperature (160 °C), where the background signal

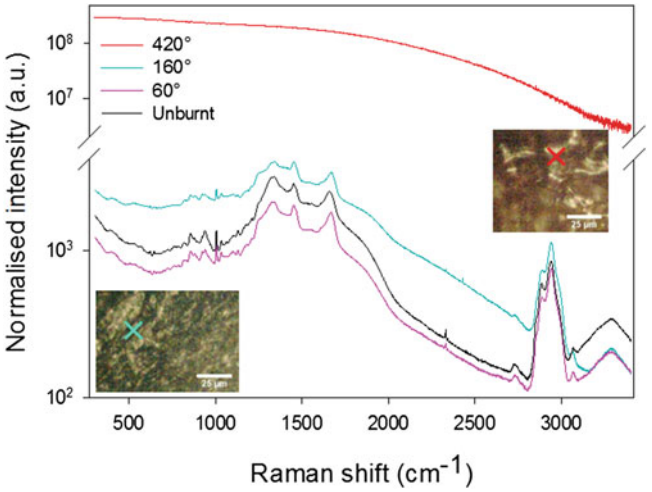


**Fig. 6.7** Raman spectra of porcine skin heated to 60, 160 and 420 °C and skin which has not been burnt. Spectra have been normalised according to the laser power used for acquisition. An exposure time of 10 s to the Raman excitation laser beam was used for acquisition of all spectra. Insets show the appearance of the skin after burning at 160 and 420 °C with *cyan* and *red crosses* respectively identifying the area from which the spectrum was acquired. Scale bars are 25 μm

was still higher than that of unburnt skin. The fluorescence observed in burnt skin is thought to arise from the denaturation of collagen or other cellular proteins during heating [18].

The ability of Raman spectroscopy to identify thermal damage is again shown in the variation of spectra with increasing distance from a burnt area (Fig. 6.8). Fluorescence decreases and characteristic skin spectral features become increasingly apparent further from the burnt site. Raman spectroscopy is therefore an effective tool to determine the extent of the damage to tissue after laser poration.

### *6.2.2 Comparison of Pores in Inked and Uninked Skin*

Raman spectra from the bottom of pores produced using the lens set-up in both uninked and inked skin, with depths of 300 and 120 μm, respectively, were acquired (Fig. 6.9). In uninked skin, the spectrum from the bottom of the pore shows a high background fluorescence and lack of characteristic spectral features. The spectrum is similar to that of skin burnt at 420 °C (Fig. 6.7), suggesting that the pore has been burnt, consistent with optical microscope images (Fig. 6.1). The spectrum of the skin at the bottom of the pore in inked skin is approximately 50 times lower in intensity than that in uninked skin, suggesting low thermal damage. Characteristic spectral

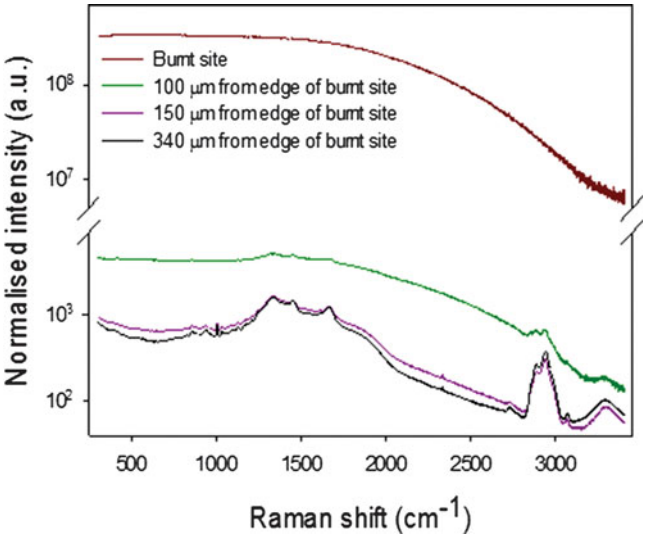


**Fig. 6.8** Raman spectra as a function of distance from an area of porcine skin heated to 420 °C. Spectra have been normalised according to the laser power used for acquisition. Exposure times of 12 s to the Raman excitation laser beam were used for all spectra

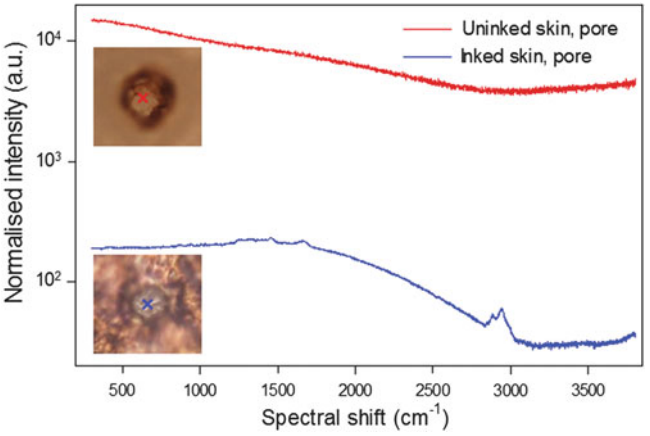


**Fig. 6.9** Raman spectra of the *bottom* of laser pores produced in uninked (*red line*) and inked (*blue line*) skin. Powers of 1.3 and 0.7 W were used for poration, respectively. Spectra have been normalised according to the laser power used for their acquisition (0.5 and 100 % of the maximum power available for uninked and inked skin, respectively) using the Raman microscope. An exposure time of 120 s was used for acquisition of Raman spectra. *Insets*: optical images with *red* and *blue crosses* show the positions from which spectra were taken in uninked and inked skin, respectively

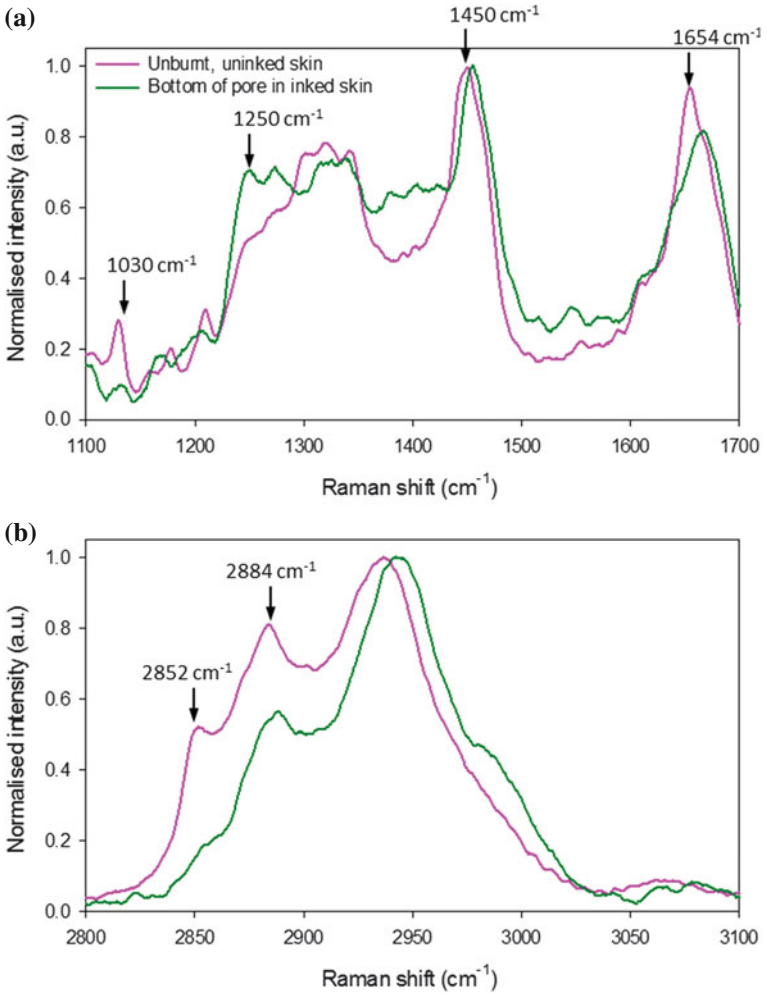


**Fig. 6.10** Raman spectra of unburnt, uninked skin (*pink*) and of the *bottom* of a pore in inked skin (*green*). Background fluorescence has been subtracted to better compare the spectra. The spectrum from the bottom of the pore has been smoothed. Spectra have been normalised according to the maximum intensity within the ranges shown: **a** 1100–1700 $cm^{-1}$ and **b** 2800–3100 $cm^{-1}$. *Arrows* indicate spectral features of interest

peaks are also visible. This effect was observed for spectra of three pores in both inked and uninked skin.

The fluorescent background was subtracted from the spectrum of the bottom of the pore in inked skin and the resulting difference was compared to that of uninked, undamaged skin (Fig. 6.10). The following observations were made: a decrease in the intensity of peaks related to the conformational order of the lipids within the skin (peaks at 1130, 2852 and 2884 $cm^{-1}$), shifts of peaks associated with the scissoring

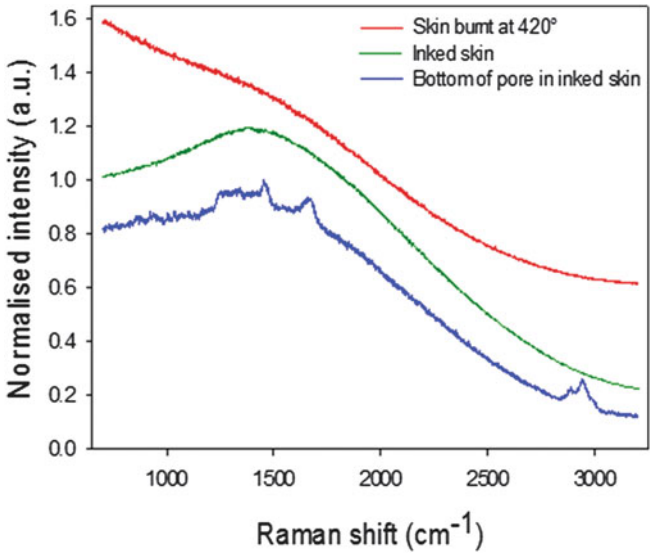


**Fig. 6.11** Raman spectra of porcine skin which was heated to 420 °C (*red line*), which was inked and not heated (*green*) and which was inked then porated (*blue*). Spectra have been normalised according to maximum intensity and offset for comparison

of $CH_2$ and C = 0 bond stretching (1450–1456 and 1654–1670 $cm^{-1}$, respectively), and the appearance of a new peak at 1250 $cm^{-1}$ assigned to the $CH_2$ bond wagging [19]. Previously recorded spectra of undamaged skin from locations beneath the SC show similar features [19]. It follows that, in this case, laser poration of the skin has caused little thermal damage.

The fluorescence observed in the Raman spectrum of the bottom of the pore in inked skin may, in fact, be due to the ink. Spectra of unburnt, inked skin and skin burnt at 420 °C (Fig. 6.11) show differences in the fluorescence from these two samples. The spectral shape of the fluorescence arising from ink agrees more closely with the spectrum from the pore in inked skin than the spectrum from burnt skin. This implies that the fluorescence observed in the pore may arise from residual ink, as opposed to thermal damage.

The difference between the Raman spectra of pores produced in uninked and inked skin may be due to the lower power used to produce the pore in inked skin and/or the effect of the ink on the poration mechanism. The presence of the ink permits poration to be achieved at lower power than in uninked skin. Regardless of whether the extent of thermal damage arises from the presence of the ink or from the power used, there is less thermal damage in the pore produced in inked skin. Using the fibre set-up allows even lower powers to be used to porate the skin, which would result in further reduced thermal damage.

## 6.3 Permeation Enhancement

To determine whether the pores created using femtosecond laser pulses would facilitate delivery in inked skin, the permeation of caffeine was investigated. Arrays of $18 \times 18$ pores in inked skin were produced at 0.06 and 0.3 W (Fig. 6.12) (low and high power, respectively). The diameters of the pores were $39 \pm 5$ and $52 \pm 12$ μm, and the distances between the pores were $130 \pm 8$ and $135 \pm 18$ μm for low and high power, respectively. The depths of these pores were not measured as this would have caused too great a delay between pore creation and the start of the permeation experiments. However, based on previous experiments (Fig. 6.3), it is likely that the depths of pores produced at high and low laser powers were approximately 50 and 15 μm, respectively.

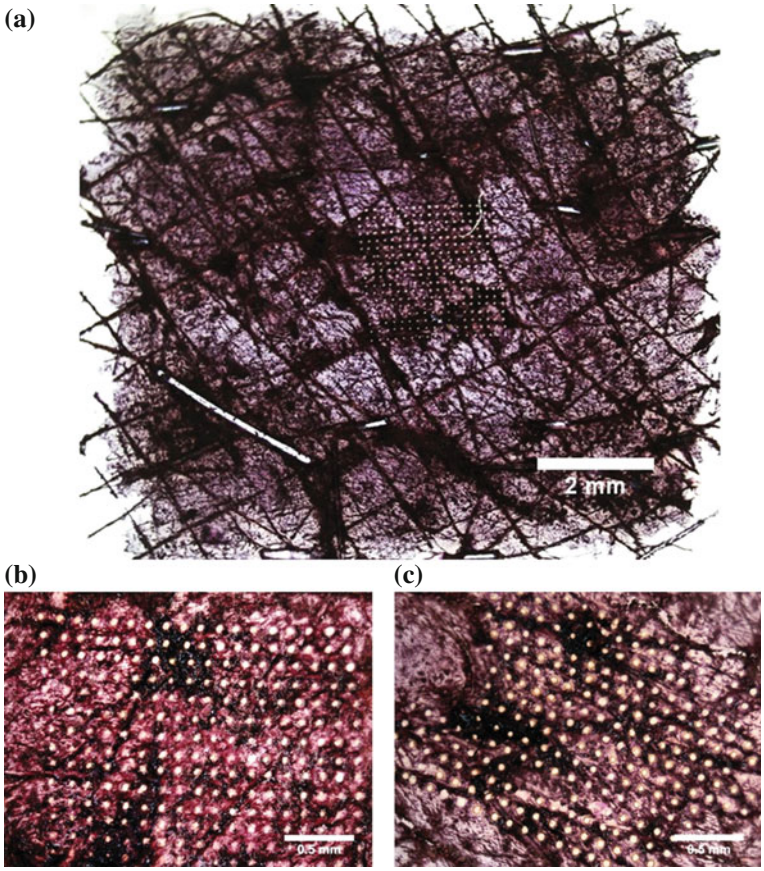


**Fig. 6.12** Optical images of laser pores produced in inked porcine skin: **a** an $18 \times 18$ array of pores produced at a laser power of 0.06 W, **b** higher magnification of the previous image, **c** pores produced at a laser power of 0.30 W. Scale bars for **b** and **c** represent 0.5 mm

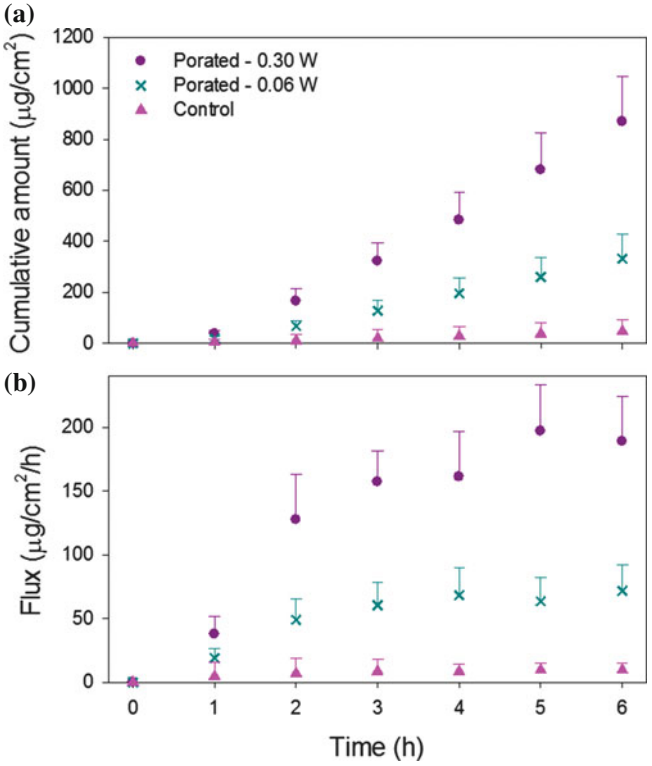


**Fig. 6.13** Permeation profiles of caffeine across intact porcine skin (n = 6) and skin porated laser powers of 0.06 (n = 3) and 0.30 W (n = 3): **a** cumulative amount permeated, and **b** flux as a function of time

The cumulative passive permeation of caffeine across non-porated skin (Fig. 6.13) after 6 h was 48 ± 44 μg $cm^{-2}$. Laser poration elicited a significant enhancement, increasing the cumulative amounts of caffeine delivered to 330 ± 100 and 870 ± 180 μg $cm^{-2}$ for low power and high power, i.e., an enhancement factor of 7 for low power and 18 for high. The flux of caffeine through the porated skin after 6 h is 7.5 and 19.9 times greater than that through non-porated skin for low and high power, respectively. The corresponding flux increases quickly with time then begins to plateau at approximately 50 and 200 μg $cm^{-2}$ $h^{-1}$.

The total area of poration produced at higher power was approximately 1.8 times greater than that at lower power. The difference in caffeine permeation between high and low power is likely due to the larger areas of the pores, as well their greater depth, when using higher power. The difference is not exactly proportional to the areas of the pores, probably because complete disruption of the SC was not achieved in all pores. As permeation increases with higher laser power, it is likely that little thermal damage, and therefore very little coagulation, has occurred, in contrast to earlier observations using older laser models [20].

## 6.4 Mechanism of Ablation

Due to the ultrashort (femtosecond) pulse durations used in these experiments, it is likely that the mechanism of skin poration is plasma-mediated ablation [21], in which the plasma is formed by laser induced breakdown of the tissue. Within the plasma volume, tissue vaporization and disintegration occurs [14]. For breakdown and plasma formation to occur in tissue, a threshold free electron density must be reached [22] (see Sect. 2.4.2). The presence of a threshold of poration, as shown in Fig. 6.3, is a result of this minimum electron density requirement for laser induced breakdown of the skin; the parameters of the laser irradiation must be such that the electron density builds up despite the loss of free electrons through diffusion and recombination, and loss of energy through collisions with ions [14]. This critical density can be produced by avalanche ionization and multiphoton ionization [14].

It has been shown that the optical breakdown in water is similar to that in transparent biological media [14]. The rate of pure multiphoton ionization of water is independent of the number of free "seed" electrons, as each atom is independently ionized [14, 22] and multiphoton ionization is independent of the linear absorption coefficient [23]. As the thresholds found in these experiments vary according to the presence of ink, it is likely, therefore, that laser induced breakdown occurs via avalanche ionization, as opposed to multiphoton. The laser radiation is absorbed by the black ink, resulting in thermionic emission of free electrons [14]. Once the irradiance is high enough to produce a seed electron, the necessary density of electrons for laser induced breakdown is rapidly reached. This effect has previously been studied in dye-enhanced pulsed laser ablation of enamel [23].

In uninked skin, seed electrons for breakdown may arise from impurities within the skin or chromophores which are absorbant at the laser wavelength (532 nm in this case) such as melanin. There may also be multiphoton initiated avalanche ionization. This also occurs in the presence of ink, but in that case, ionization due to the seed electrons would dominate. The absorption of laser radiation by uninked skin is much lower. A higher fluence is therefore required to ensure that a threshold electron density is achieved. The greater fluence required results in more collateral thermal damage in the surrounding tissue [24], and is consistent with the greater thermal damage observed using Raman spectroscopy (Fig. 6.9).

By increasing the laser power for poration, a greater area of the beam (at a given distance from the lens focal point or the end of the fibre) has a fluence large enough for ablation (inset of Fig. 6.3) and therefore larger pores are produced. This also explains the increasing diameters of the pores with greater distances between the fibre and the skin (Fig. 6.5); the width of the Gaussian beam increases with distance from the end of the fibre. For the data shown in Fig. 6.5, the fluence was great enough to cause poration at all distances investigated and the diameter increased with increasing distance. It is likely that, beyond a certain distance, a greater proportion of the beam will be below the threshold fluence and the diameter of the pores would then decrease with increasing distance.

Pores were shallower when produced with lower laser powers/fluences (Fig. 6.3) but the variation in depth is less pronounced at lower powers. At higher fibre-skin distances, it would be expected that the depth of the pores created would be shallower due to the decrease in fluence. Although this relation was not observed here at the powers used with the fibre set-up (Fig. 6.5), the absence of an observable trend may be due to the measurement difficulties, discussed in Sect. 6.1.4, or by the diminishing influence of the ink as the pores become deeper. The explosive ejection of the plasma per pulse would leave some material at the edges and at the bottom of the produced pore. Some of this material is likely to contain some of the absorbent ink. Its effect on the initiation of a plasma would therefore translate to lower depths with decreasing influence. Once the influence of the ink is removed, ablation is no longer possible and poration ceases.

Pores in inked and uninked skin have the same diameter and depth when produced at the same laser power above 0.7 W (Fig. 6.3). Under these conditions, a different mechanism of poration may dominate where the bulk material properties have a greater influence on poration than the surface ink. For example, the ink may be rapidly removed at these powers and the poration is achieved by the interaction of the laser radiation with uninked skin.

In the plasma mediated ablation of enamel, it was found that the ablation depth increased with each pulse [24]. In our work on inked skin, ablation depth and diameter show no relation with increasing pulse number (exposure time) (Fig. 6.6). This may be because the poration process stops at times less than the minimum used (0.07 s). Once the influence of the ink is removed, uninked skin remains that does not porate at the fluences used on inked skin. The poration process therefore stops.

## 6.5 Summary and Conclusions

Femtosecond pulsed laser radiation has been used to porate porcine skin and to enhance drug permeation. The application of ink to the surface of the skin lowered the power required to porate the skin. The lower powers resulted in less thermal damage, as determined using Raman spectroscopy, to the tissue surrounding the pores. This was beneficial for enhancing drug permeation as little coagulation occurred to provide a barrier to penetration.

The laser beam was focussed on or directed at the skin using either a lens or a fibre. The threshold for poration was lowest in inked skin when the fibre set-up was used. The effect of laser power, exposure time and distance between the end of the fibre and the skin on pore dimensions was attributed to the beam propagation and plasma-mediated mechanism of ablation.

This method of poration presents the following advantages over the more frequently used ablation using longer pulses, which rely on photothermal ablation and the strong absorption of the laser wavelength by water. The short pulse durations used in these experiments and the incidence of poration at low fluences ensured that there was little damage to the surrounding tissue. The use of a fibre laser and a fibre

to direct the light towards the skin also increases the flexibility of the system and renders a putative poration device more compact and portable. While photothermal ablation is more efficient for strongly absorbing tissues [23], femtosecond ablation is independent of the natural variations in the tissue properties, a particular advantage given the structural heterogeneity of skin. However, femtosecond pulsed lasers are expensive. Once the technology has developed and components become more readily available, femtosecond ablation could provide an advantageous alternative to that currently used. This kind of ablation may also prove promising in applications such as damage-free separation of tissue, for example, for skin grafts [10], and for drug delivery into the nail [25].

## References

1. R. Weiss, M. Hessenberger, S. Kitzmuller, D. Bach, E.E. Weinberger, W.D. Krautgartner, C. Hauser-Kronberger, B. Malissen, C. Boehler, Y.N. Kalia, J. Thalhamer, S. Scheiblhofer, Transcutaneous vaccination via laser microporation. J. Controlled Release **162**(2), 391–399 (2012)
2. Y.G. Bachhav, A. Heinrich, Y.N. Kalia, Controlled intra- and transdermal protein delivery using a minimally invasive erbium:yag fractional laser ablation technology. Eur. J. Pharm. Biopharm. **84**(2), 355–364 (2013)
3. X.Y. Chen, D. Shah, G. Kositratna, D. Manstein, R.R. Anderson, M.X. Wu, Facilitation of transcutaneous drug delivery and vaccine immunization by a safe laser technology. J. Controlled Release **159**(1), 43–51 (2012)
4. W.R. Lee, S.C. Shen, M.H. Pai, H.H. Yang, C.Y. Yuan, J.Y. Fang, Fractional laser as a tool to enhance the skin permeation of 5-aminolevulinic acid with minimal skin disruption: A comparison with conventional erbium:yag laser. J. Controlled Release **145**(2), 124–133 (2010)
5. E.M. Graber, E.L. Tanzi, T.S. Alster, Side effects and complications of fractional laser photothermolysis: experience with 961 treatments. Dermatol. Surg. **34**(3), 301–307 (2008)
6. C. Gomez, A. Costela, I. Garcia-Moreno, F. Llanes, J.M. Teijon, D. Blanco, Laser treatments on skin enhancing and controlling transdermal delivery of 5-fluorouracil. Lasers Surg. Med. **40**(1), 6–12 (2008)
7. C. Gomez, A. Costela, I. Garcia-Moreno, F. Llanes, J.M. Teijon, M.D. Blanco, Skin laser treatments enhancing transdermal delivery of ala. J. Pharm. Sci. **100**(1), 223–231 (2011)
8. G. Nicolodelli, D.P. Angarita, N.M. Inada, L.F. Tirapelli, V.S. Bagnato, Effect of photodynamic therapy on the skin using the ultrashort laser ablation. J. Biophotonics (2013)
9. K.S. Frederickson, W.E. White, R.G. Wheeland, D.R. Slaughter, Precise ablation of skin with reduced collateral damage using the femtosecond-pulsed, terawatt titanium-sapphire laser. Arch. Dermatol. **129**(8), 989–993 (1993)
10. H. Huang, Z.X. Guo, Human dermis separation via ultra-short pulsed laser plasma-mediated ablation. J. Phys. D-Appl. Phys. **42**(16) (2009)
11. G. Humbert, J.C. Knight, G. Bouwmans, P.S. Russell, D.P. Williams, P.J. Roberts, B.J. Mangan, Hollow core photonic crystal fibers for beam delivery. Opt. Express **12**(8), 1477–1484 (2004)
12. R. Paschotta, *Encyclopedia of laser physics and technology* (Wiley-VCH, Weinheim, 2008)
13. L. Tchvialeva, H. Zeng, I. Markhvida, D.I. McLean, H. Lui, T.K. Lee, Skin Roughness Assessment. InTech (2010)
14. A. Vogel, V. Venugopalan, Mechanisms of pulsed laser ablation of biological tissues. Chem. Rev. **103**(2), 577–644 (2003)
15. Y.G. Bachhav, S. Summer, A. Heinrich, T. Bragagna, C. Bohler, Y.N. Kalia, Effect of controlled laser microporation on drug transport kinetics into and across the skin. J. Controlled Release **146**(1), 31–36 (2010)

16. J. Yu, Y.G. Bachhav, S. Summer, A. Heinrich, T. Bragagna, C. Bohler, Y.N. Kalia, Using controlled laser-microporation to increase transdermal delivery of prednisone. J. Controlled Release **148**(1), E71–E73 (2010)
17. E.H. Taudorf, C.S. Haak, A.M. Erlendsson, P.A. Philipsen, R.R. Anderson, U. Paasch, M. Haedersdal, Fractional ablative erbium yag laser: histological characterization of relationships between laser settings and micropore dimensions. Lasers Surg. Med. **46**(4), 281–289 (2014)
18. N. Iftimia, R.D. Ferguson, M. Mujat, A.H. Patel, E.Z. Zhang, W. Fox, M. Rajadhyaksha, Combined reflectance confocal microscopy/optical coherence tomography imaging for skin burn assessment. Biomed. Opt. Express **4**(5), 680–695 (2013)
19. C.H. Xiao, C.R. Flach, C. Marcott, R. Mendelsohn, Uncertainties in depth determination and comparison of multivariate with univariate analysis in confocal raman studies of a laminated polymer and skin. Appl. Spectrosc. **58**(4), 382–389 (2004)
20. S.L. Jacques, D.J. Mcauliffe, I.H. Blank, J.A. Parrish, Controlled removal of human stratum-corneum by pulsed laser. J. Invest. Dermatol. **88**(1), 88–93 (1987)
21. X.H. Hu, Q.Y. Fang, M.J. Cariveau, X.N. Pan, G.W. Kalmus, Mechanism study of porcine skin ablation by nanosecond laser pulses at 1064, 532, 266, and 213 nm. IEEE J. Quantum Electron. **37**(3), 322–328 (2001)
22. D.X. Hammer, R.J. Thomas, G.D. Noojin, B.A. Rockwell, P.K. Kennedy, W.P. Roach, Experimental investigation of ultrashort pulse laser-induced breakdown thresholds in aqueous media. IEEE J. Quantum Electron. **32**(4), 670–678 (1996)
23. A.A. Oraevsky, L.B. DaSilva, A.M. Rubenchik, M.D. Feit, M.E. Glinsky, M.D. Perry, B.M. Mammini, W. Small, B.C. Stuart, Plasma mediated ablation of biological tissues with nanosecond-to-femtosecond laser pulses: relative role of linear and nonlinear absorption. IEEE J. Sel. Top. Quantum Electron. **2**(4), 801–809 (1996)
24. R. Esenaliev, A. Oraevsky, S. Rastegar, C. Frederickson, M. Motamedi, Mechanism of dye-enhanced pulsed laser ablation of hard tissues: Implications for dentistry. IEEE J. Sel. Top. Quantum Electron. **2**(4), 836–846 (1996)
25. J. Neev, J.S. Nelson, M. Critelli, J.L. McCullough, E. Cheung, W.A. Carrasco, A.M. Rubenchik, L.B. DaSilva, M.D. Perry, B.C. Stuart, Ablation of human nail by pulsed lasers. Lasers Surg. Med. **21**(2), 186–192 (1997)